Journal of Photochemistry and Photobiology A: Chemistry 223 (2011) 97–102

Contents lists available at ScienceDirect

Journal of Photochemistry and Photobiology A: Chemistry

journal homepage: www.elsevier.com/locate/jphotochem

Facile fabrication of polypyrrole/functionalized multiwalled carbon nanotubes composite as counter electrodes in low-cost dye-sensitized solar cells

Shengjie Peng[a,c,*], Yongzhi Wu[b,c], Peining Zhu[c], Velmurugan Thavasi[c], Subodh G. Mhaisalkar[a], Seeram Ramakrishna[c,d,e,*,1]

[a] School of Materials Science and Engineering, Nanyang Technological University, Singapore 639798, Singapore
[b] NUS Graduate School for Integrative Sciences and Engineering, National University of Singapore, Singapore 117456, Singapore
[c] Healthcare and Energy Materials Laboratory, NUS Nanoscience and Nanotechnology Initiative, National University of Singapore, Singapore 117576, Singapore
[d] Institute of Materials Research and Engineering, Singapore 117602, Singapore
[e] King Saud University, 11451 Riyadh, Saudi Arabia

ARTICLE INFO

Article history:
Received 7 May 2011
Received in revised form 27 July 2011
Accepted 11 August 2011
Available online 19 August 2011

Keywords:
Dye-sensitized solar cells
Counter electrodes
Flexible substrates
Carbon nanotube
Polypyrrole

ABSTRACT

This paper reports facile fabrication of polypyrrole (Ppy)/functionalized multiwalled carbon nanotube (*f*-MWCNT) nanocomposite films on rigid fluorine-doped tin oxide (FTO) and flexible ITO-coated polyethylene naphthalate (PEN) substrates by a drop casting method, and their application as counter electrodes in dye-sensitized solar cells (DSSCs). The electrochemical impedance spectroscopy (EIS) and cyclic voltammetry (CV) measurements of this solution processed Ppy/*f*-MWCNT nanocomposite film display good catalytic performance for I_3^-/I^- solution. The photoelectric conversion efficiency of the DSSCs with the Ppy/*f*-MWCNT counter electrodes on FTO and PEN substrates reaches 7.02% and 4.04%, respectively, under AM1.5 illumination of 100 mW cm^{-2}, comparable to that of the DSSCs based on sputtered Pt electrodes. The fabrication method of such counter electrodes is simple under room temperature and can be applicable in large-scale production.

1. Introduction

In recent years, dye-sensitized solar cells (DSSCs) have received much attention as an alternative to silicon-based solar cells due to their low-cost fabrication and relatively high conversion efficiency [1]. In general, the DSSCs are made up of nanocrystalline TiO_2 electrode, Ru-based dye, electrolyte containing a redox couple (I_3^-/I^-), and Pt electrode. The Pt counter electrode is an indispensable component in a DSSC and its role is to transfer electrons from the external circuit back to the redox electrolyte, and to catalyze the reduction of the redox couple for sustaining low overvoltage. Conventional Pt counter electrodes are often obtained by thermal decomposition, sputtering, and electrodeposition [2–4]. However, the high price of Pt and the usage of complex equipment are the serious drawbacks in large-scale and cost-effective fabrication of DSSCs. In particular, the most common thermal decomposition process for Pt films is not applicable for making flexible DSSCs, due to the high temperature requirement for the fabrication process. Therefore, great efforts have been ongoing currently to develop lower cost and higher efficient counter electrodes for rigid and flexible DSSCs, such as sulfides, nitrides and carbon materials [5–7].

Conductive polymers are very promising alternatives for counter electrode materials in DSSCs because of their unique properties such as affordability, good stability, and higher catalytic activity for I_3^- reduction [8–10]. Polypyrrole (Ppy), as a typical conductive polymer, has been intensively studied; however, it suffered from relatively lower conductivity that would directly affect the performance of the device [9]. Polypyrrole has been prepared on FTO substrates by electrodeposition, which exhibited good electrocatalytic performance [10]. Besides the conductive polymers, carbon materials have also been explored to replace Pt and showed good performance due to their high surface area and electronic conductivity to redress their intrinsic poor electrochemical catalytic activity [11,12]. Furthermore, multiwalled carbon nanotubes (MWCNTs) have been well known for their fast electron-transport architecture, which also possess an electrocatalytic activity for the I_3^- reduction in the electrolyte [13]. Another advantage is that functionalized multiwalled carbon nanotubes (*f*-MWCNTs) can be easily dispersed in water by functionalizing the surface of MWCNTs, offering low toxicity and environment friendly characters.

* Corresponding authors at: Healthcare and Energy Materials Laboratory, NUS Nanoscience and Nanotechnology Initiative, National University of Singapore, Singapore 117576, Singapore. Tel.: +65 98602569.
E-mail addresses: sjpeng@ntu.edu.sg (S. Peng), seeram@nus.edu.sg (S. Ramakrishna).
[1] .Tel.: +65 65166593.

1010-6030/$ – see front matter © 2011 Elsevier B.V. All rights reserved.
doi:10.1016/j.jphotochem.2011.08.004

The superior catalytic performance of Ppy can interact with high electrical conductive *f*-MWCNTs to enhance their solubility in the solution and form thin films easily by a simple and low-cost drop casting technique. In this paper, homogeneous and well adhesive Ppy/*f*-MWCNT films are successfully fabricated on FTO and also PEN substrates at room temperature. The Ppy/*f*-MWCNT composite films demonstrate lower electron transfer resistance and superior solar cell performance in rigid and flexible DSSCs, respectively, indicating efficient counter electrodes in DSSCs.

2. Experimental details

2.1. Materials

Polypyrrole aqueous solution (Ppy, 5 wt% dispersion in H_2O, conductivity >0.05 S m^{-1}, Sigma–Aldrich), multiwalled carbon nanotubes (MWCNTs, Shenzhen Nanotech Port Co. Ltd., China), fluorine-doped tin oxide (FTO, 8–12 Ω sq^{-1}, Sigma–Aldrich), ITO-coated polyethylene naphthalate (PEN, 8–12 Ω sq^{-1}, Sigma–Aldrich), TiO_2 paste (Solaronix), and TiO_2 (P25, Degussa AG, Germany, a mixture of ca. 30% rutile and 70% anatase), the dye, cis-diisothiocyanato-bis(2,2-bipyridyl-4,4-dicarboxylato) ruthenium(II) bis (tetrabutylammonium) (N719, Solaronix) and titanium(IV) isopropoxide (TTIP, Sigma–Aldrich, 99.999%).

2.2. Fabrication Ppy/f-MWCNT counter electrodes

Ppy/*f*-MWCNT films on FTO and PEN substrates were fabricated by functionalizing MWCNTs, followed by drop casting the Ppy/*f*-MWCNT aqueous solution. First, 200 mg of the pristine MWCNTs were dispersed in 200 ml of concentrated H_2SO_4:HNO_3 (3:1) solution and refluxed at 90 °C for 1 h. This step enabled the functionalization of MWCNTs with carboxylic acid groups [14]. Second, 10 mg of the treated *f*-MWCNTs and 20 mL of 0.05% Ppy aqueous solution were mixed under ultrasonification for 30 min in order to form a stable dispersion aqueous solution. Then, several drops were cast on the FTO or PEN substrates; the resultant black films were dried at 60 °C under vacuum, and then employed as the counter electrodes in DSSCs. The thickness of films could be controlled by adjusting the concentration and the amount of precursor composite solution. For comparison purpose, Ppy and *f*-MWCNTs films were prepared as the counter electrodes by similar drop casting their aqueous dispersion, respectively, and Pt counter electrodes were obtained by sputtering.

2.3. Fabrication of TiO_2 electrodes on FTO and PEN substrates

The TiO_2 films on FTO glass with a thickness of 15 μm were prepared by using screen printing and doctor blade techniques with standard TiO_2 paste (Solaronix), and then they were heated at 450 °C for 30 min. For the flexible DSSCs, FTO substrates were replaced by PEN. The TiO_2 paste was fabricated by mixing the P25 nanoparticles, TTIP and ethanol as reported in the literature [15]. The procedure of the TiO_2 on PEN substrates was similar to that on FTO glass.

2.4. Assembly of DSSCs

DSSCs were assembled by employing N719-sensitized nanoporous TiO_2 electrodes and the Ppy/*f*-MWCNT counter electrodes, as shown in Fig. 1. The liquid electrolyte, which was a mixture of 0.6 M DMPImI, 0.1 M LiI, 0.05 M I_2, t-butylpyridine and acetonitrile solvent, was dropped onto the nanoporous TiO_2 film, and then the TiO_2 electrode was clipped firmly with the counter electrode. The active area of the DSSCs was 0.16 cm^2.

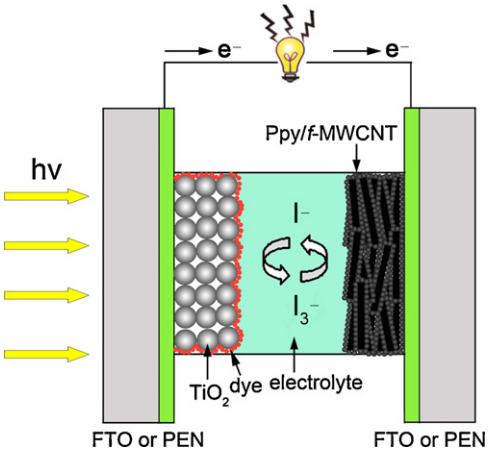

Fig. 1. Schematic illustration of the cross-sectional view for the DSSC with the TiO_2 electrode and the Ppy/*f*-MWCNT counter electrode on the FTO or PEN substrate.

2.5. Characterization of samples and DSSCs

The morphologies of the as-obtained Ppy/*f*-MWCNT were investigated by using scanning electron microscopy (SEM, JEOL JSM-6701F) and high resolution transmission electron microscopy (HRTEM, JEOL 3010). SEM and HRTEM were operated at 30 kV and 300 kV, respectively. The infrared (IR) spectra were recorded in the wavenumber range of 4000–500 cm^{-1} with a Nicolet Model 759 Fourier transform infrared (FTIR) spectrometer. Electrochemical impedance spectroscopy (EIS) measurement of two identical counter electrodes was conducted with an impedance analyzer Parstat 2273, Princeton, at zero bias potential and 10 mV of amplitude over the frequency range of 0.1 Hz–100 kHz. Cyclic voltammetry (CV) measurement was carried out in a N_2-purged acetonitrile solution at a different scan rate (20–100 mV s^{-1}). The counter electrode, a Pt coil and an Ag/Ag^+ electrode were used as the photocathode, the working electrode, and the reference electrode, respectively. The electrolyte was the acetonitrile solution containing 0.1 mol L^{-1} $LiClO_4$ as the supporting electrolyte and 10 mmol L^{-1} LiI + 1 mmol L^{-1} I_2 as the redox couple. Photocurrent–voltage curves were carried out using a XES-151 S solar simulator (San-Ei, Japan) under AM1.5 condition. The level of standard irradiance (1 Sun conditions, 100 mW cm^{-2}) was set with a calibrated c-Si reference solar cell.

3. Results and discussion

3.1. Morphologies and IR measurement

Fig. 2 shows SEM images of Ppy/*f*-MWCNT film, and HRTEM image of Ppy/*f*-MWCNT. As can be seen from Fig. 2(a) and (b), one-dimensional structure of *f*-MWCNTs was not damaged by introducing Ppy, and a uniform Ppy/*f*-MWCNT film with a thickness of about 3 μm was found to be covered the FTO glass. The HRTEM image in Fig. 2(c) demonstrates that the external surface of the composite is rough and Ppy nanoparticles with an average size of about 2 nm are found to be adhered on the surface of the *f*-MWCNT. It is believed that *f*-MWCNTs act as a template, and absorb Ppy nanoparticles to form Ppy/*f*-MWCNT composite due to possible interactions between Ppy and *f*-MWCNTs [16].

Fig. 3 displays the FTIR spectra of *f*-MWCNTs, Ppy, and Ppy/*f*-MWCNT. It can be seen that the peak at 1702 cm^{-1} and 1205 cm^{-1} can be assigned to the C=O stretch and C–O bend, indicating the formation of the COOH groups on the MWCNT [17]. In the case of Ppy, the main characteristic peak at 1556 cm^{-1} may be assigned to typical polypyrrole ring vibrations [18]. The band

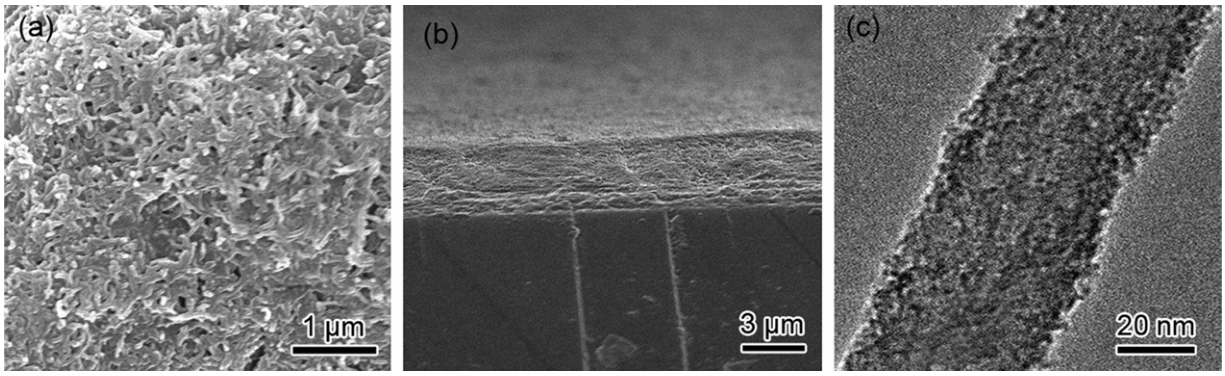

Fig. 2. SEM images of the surface (a) and cross section (b) of Ppy/*f*-MWCNT film, and HRTEM image (c) of Ppy/*f*-MWCNT nanocomposite.

at 1036 cm^{-1} corresponds to the N–H in-plane deformation. The peaks at 1210 cm^{-1} and 914 cm^{-1} may be assigned to N–C stretching band and C–H band. It is found that all the above characteristic peaks of Ppy are also observed in the spectrum of the Ppy/*f*-MWCNT nanocomposite, but some peaks have a little shift and the intensity is enhanced; so it can be proved that there are interactions (probably π–π noncovalent bonds) between Ppy and *f*-MWCNTs [18]. And these interactions can make electron transport between Ppy and *f*-MWCNTs occur easily.

3.2. Electrochemical measurement

EIS analysis was carried out to understand the catalytic performance of the counter electrodes. Fig. 4(a) and (b) shows the Nyquist plots of the symmetrical *f*-MWCNTs, Ppy, Ppy/*f*-MWCNT, and Pt films on FTO glass substrates, and their equivalent circuit for the impedance spectra (inset in Fig. 4(b)). In the Nyquist plot, the semicircle at the high frequency range corresponds to the charge-transfer resistance (R_{ct}) of the counter electrode, which describes catalytic activity for reducing triiodide ions, whereas the semicircle at low frequency side represents diffusion impedance (Z_w) of the I_3^-/I^- redox couple in the electrolyte [19,20]. The R_{ct} of 26.17 Ω cm^2, 19.94 Ω cm^2, 1.81 Ω cm^2, and 2.69 Ω cm^2 can be deduced for *f*-MWCNTs, Ppy, Ppy/*f*-MWCNT and Pt films, respectively. The obtained R_{ct} value of Ppy/*f*-MWCNT electrode is found to be much lower than those of PPy and *f*-MWCNTs electrodes, and even lower than that in the case of Pt film, indicating a higher catalytic performance characteristic of Ppy/*f*-MWCNT, which is due to the high electrical conductivity and superior electrocatalytic activity of Ppy/*f*-MWCNTs electrode (Table 1). As *f*-MWCNTs with a high surface area and Ppy nanoparticles can provide fast electron-transport channels and plenty of interfacial active sites, this network structure demonstrates an ideal counter electrode material due to the interaction of π–π coupling between them characterized by the IR measurement, when *f*-MWCNTs are coated by Ppy nanoparticles. The ohmic series resistance (R_s) can be determined by estimating the location of the intersection point of the abscissa axis of the Nyquist plots on the high frequency side where the phase is equal to zero. Among *f*-MWCNTs, Ppy, and Ppy/*f*-

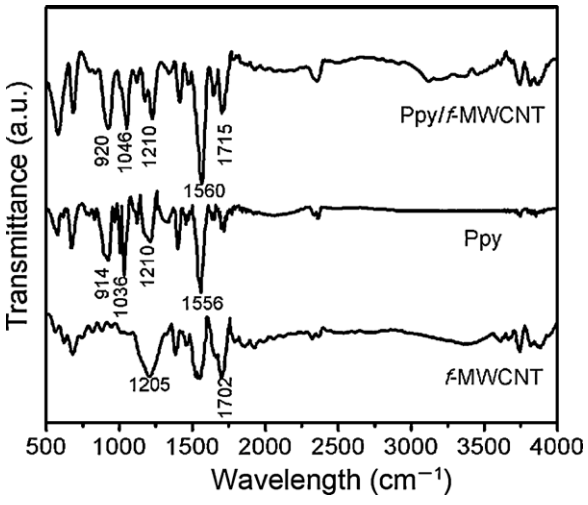

Fig. 3. FTIR spectra of the *f*-MWCNTs, Ppy, and Ppy/*f*-MWCNT films.

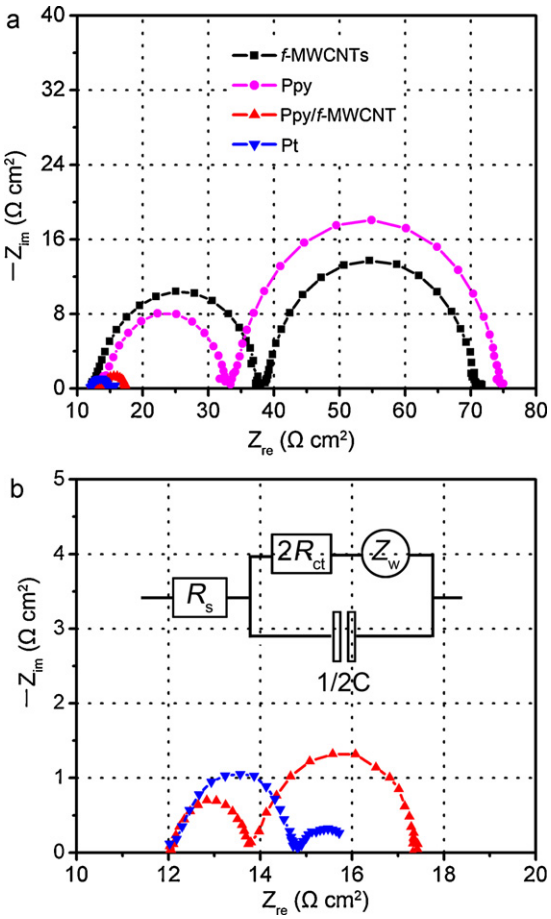

Fig. 4. Nyquist plots for the counter electrodes (*f*-MWCNTs, Ppy, Ppy/*f*-MWCNT, and Pt), respectively (a), and the magnified view for the Ppy/*f*-MWCNT and Pt counter electrode (b). Z_w, Nernst diffusion impedance; R_{ct}, charge-transfer resistance of electrode/electrolyte interface; CPE, constant phase element of electrical double layer; R_s, serial resistance. The inset shows the equivalent circuit for the impedance spectra.

Table 1
The surface area (BET) of *f*-MWCNT, PPy, and Ppy/*f*-MWCNTs powder; and electrochemical parameters of *f*-MWCNTs/FTO, Ppy/FTO, Ppy/*f*-MWCNT/FTO, and Pt/FTO electrodes.

Samples	BET ($m^2\ g^{-1}$)	Sheet resistance[a] ($\Omega\ cm^{-1}$)	R_s ($\Omega\ cm^2$)	R_{ct} ($\Omega\ cm^2$)	Z_w ($\Omega\ cm^2$)
f-MWCNTs	61.23	65.10	12.10	26.17	33.12
Ppy	25.09	198.39	13.11	19.94	40.86
Ppy/*f*-MWCNTs	71.10	48.81	12.05	1.81	3.56
Pt	–	9.32	12.00	2.69	1.41

[a] Measured by a four-point probe.

MWCNT electrodes, Ppy/*f*-MWCNT electrode shows a lower R_s value of 12.05 $\Omega\ cm^2$, and a corresponding lower sheet resistance of 48.81 $\Omega\ cm^{-1}$, which is close to that of Pt and higher than those of Ppy and *f*-MWCNT electrodes. This phenomenon is to be attributed to inherently high conducting property of Ppy/*f*-MWCNT film [21]. Also the result in Table 1 shows that the diffusion impedance of the Ppy/*f*-MWCNT is 3.56 $\Omega\ cm^2$, which is much lower than that of Ppy and *f*-MWCNT films, due to its high surface area (71.10 $m^2\ g^{-1}$) [6,22]. This result reveals that the I_3^- can be rapidly reduced to iodide ions to accelerate the diffusion of electrolyte under the catalysis of Ppy/*f*-MWCNT composite. However, the Z_w of Ppy/*f*-MWCNT is higher than that of Pt, which may be caused by a few micron thick Ppy/*f*-MWCNT film [23]. In a word, the introduction of Ppy nanoparticles on the *f*-MWCNTs not only decreases the charge-transfer resistance in the electrolyte/electrode interface, but also reduces the diffusion impedance of triiodide ions.

Cyclic voltammograms (CV) measurement was performed to analyze the relationship between ion diffusivity and reaction kinetics of an electrochemical system. Fig. 5 displays the CV curves of the *f*-MWCNTs, Ppy, Ppy/*f*-MWCNT, and Pt electrodes at a scan rate of 100 mV S^{-1} in 10 mM LiI, 1 mM I_2 acetonitrile solution containing 0.1 mol L^{-1} $LiClO_4$ as the supporting electrolyte. It can be seen that two pairs of redox peaks are observed in the CV curves. The two anode peaks correspond to the oxidation of iodide to triiodide (peak I) and then to iodine (peak II) according to the reactions;

$$3I^- \rightarrow I_3^- + 2e^- \quad (I)$$

$$2I_3^- \rightarrow 3I_2 + 2e^- \quad (II)$$

Conversely, iodine is reduced to triodide (peak I′) and then to iodide (peak II′) as follows:

$$3I_2 + 2e^- \rightarrow 2I_3^- \quad (I')$$

$$I_3^- + 2e^- \rightarrow 3I^- \quad (II')$$

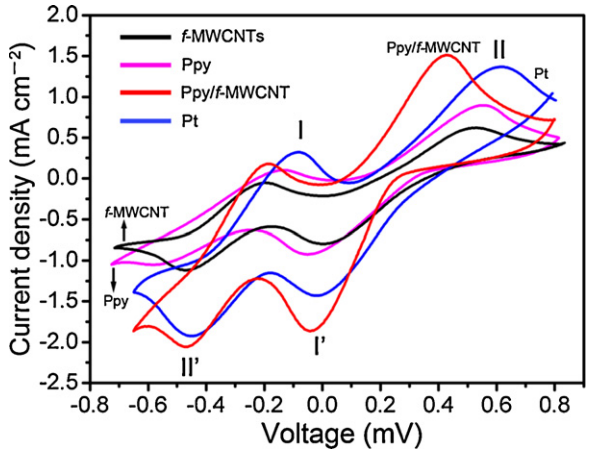

Fig. 5. Cylic voltammetry (a) for the *f*-MWCNTs, Ppy, Ppy/*f*-MWCNT, and Pt electrodes at a scan rate of 100 mV S^{-1} in 10 mM LiI, 1 mM I_2 acetonitrile solution containing 0.1 M $LiClO_4$ as the supporting electrolyte.

The Ppy/*f*-MWCNT film electrode shows the highest current density of the I_3^- reduction peak in the four film electrodes, indicating a higher catalytic reactivity on the Ppy/*f*-MWCNT electrode than that on the *f*-MWCNTs, Ppy film and Pt electrodes [19]. The sequence of the current density coincides with the charge transfer resistance R_{ct} determined from EIS tests (Fig. 4). And this higher current density of the film is advantageous for the application in DSSCs.

Fig. 6(a) illustrates cyclic voltammetry for the Ppy/*f*-MWCNT electrodes with various scan rates. It is observed that the absolute values of anodic peak currents are almost the same as those of the corresponding anodic peak currents. It can be found that the anodic peak gradually and regularly shifts towards the negative direction and the corresponding cathodic peak shifts to the positive direction with decreasing scan rate. Fig. 6(b) displays the relationship between the redox peak currents and scan rates. The good linear relationship with various scan rates indicates the diffusion limitation of the redox reaction on Ppy/*f*-MWCNT [24]. This phenomenon

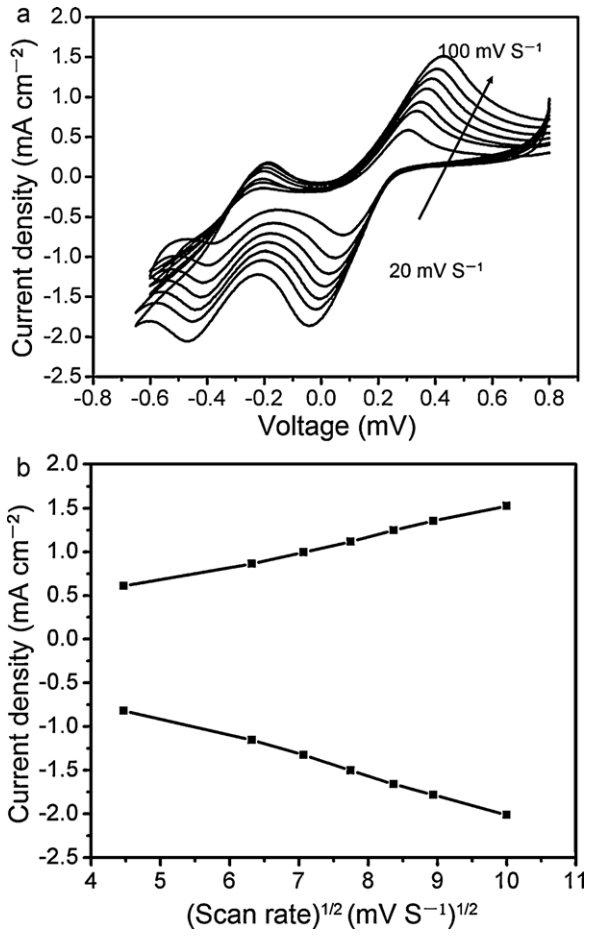

Fig. 6. Cyclic voltammetry (a) for the Ppy/*f*-MWCNT electrodes in 10 mM LiI, 1 mM I_2 acetonitrile solution containing 0.1 M $LiClO_4$ as the supporting electrolyte with different scan rates (from outer to inner: 100, 80, 70, 60, 50, 40, 20 mV s^{-1}, respectively) and the relationship (b) between the redox peak currents and scan rates.

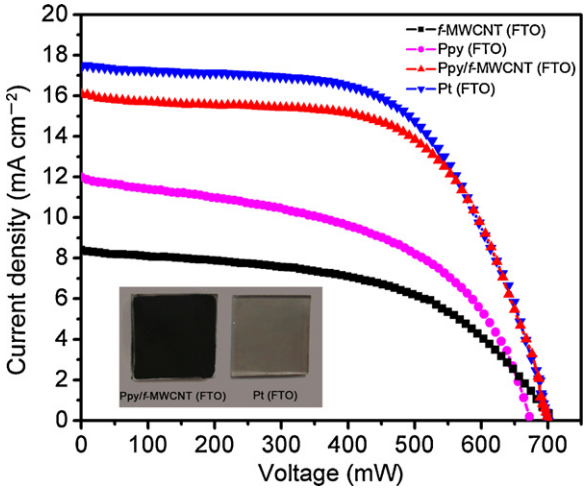

Fig. 7. Photocurrent density–voltage curves (*J*–*V*) of DSSCs with *f*-MWCNTs, Ppy, Ppy/*f*-MWCNT, Pt on FTO and PEN substrates as the counter electrodes under AM1.5 illumination of 100 mW cm^{-2}, respectively. The inset shows photos of Pt (left) and Ppy/*f*-MWCNT (right) films on FTO substrates.

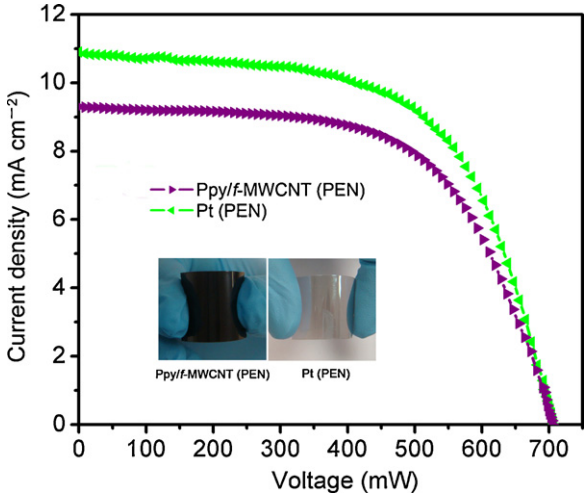

Fig. 8. Photocurrent density–voltage curves (*J*–*V*) of DSSCs with Ppy/*f*-MWCNT and Pt films on PEN substrates as the counter electrodes under AM1.5 illumination of 100 mW cm^{-2}, respectively. The inset shows photos of Pt (left) and Ppy/*f*-MWCNT (right) films on PEN substrates.

shows that the adsorption of iodide species little affects the redox reaction on the Ppy/*f*-MWCNT electrode surface, indicating no specific interaction between I_3^-/I^- redox couple and Ppy/*f*-MWCNT.

3.3. Photoelectronic application

Fig. 7 shows the photocurrent density–voltage curves of DSSCs with the configuration of *f*-MWCNTs, Ppy, Ppy/*f*-MWCNT, and Pt based films on FTO substrates, respectively, and the photos of Pt (left) and Ppy/*f*-MWCNT (right) films on FTO substrates (inset). Table 2 summarizes the photovoltaic performance of the rigid and flexible DSSCs. It can be seen that when Ppy/*f*-MWCNT composite film on FTO glass is employed as the counter electrode in DSSC, the device exhibits a voltage (V_{oc}) of 701 mV, current density (J_{sc}) of 16.1 mA cm^{-2}, fill factor (FF) of 62.1%, and an energy conversion efficiency of (η) of 7.02% under AM1.5 illumination of 100 mW cm^{-2}. This efficiency is comparable to that of sputtered Pt electrode-based DSSCs (7.55%), and much higher than that of *f*-MWCNTs (3.18%) and Ppy (4.10%) counterparts. Compared to the performance parameters obtained for DSSCs using Ppy/*f*-MWCNT and Pt electrodes (Table 2), it is observed that the Ppy/*f*-MWCNT counter electrode shows the comparable voltage and fill factor with those of the Pt electrode, while a little lower current density. The FF is generally determined by the total series resistance (R_s) of DSSCs, which can be expressed as $R_{Stot} = R_{FTO} + R_{ct} + R_{diff(I_3^-)}$ [25]. Although the R_{ct} of the Ppy/*f*-MWCNT is measured to be smaller than that of the Pt electrode, the $R_{diff(I_3^-)}$ is larger than that of the Pt electrode due to the thicker Ppy/*f*-MWCNT film, which is a trade-off of the R_{ct} [10]. Therefore, the comparable R_s matches to its corresponding FF. It is known that J_{sc} can be influenced by two main factors related to the counter electrode, internal resistance and the photo reflection properties [26,27]. The Pt electrode consists of Pt nanoclusters on the FTO substrates, which can slightly reflect the unabsorbed portion of incident solar light towards the TiO_2 photoanode. However, the black coloured Ppy/*f*-MWCNT is opaque in nature, hence it cannot involve in the reflection effect. Therefore the relatively lower J_{sc} is ascribed to the high photoabsorption ability of black carbon materials. It is believed that good photovoltaic performance of Ppy/*f*-MWCNT is attributed to the π–π coupling and cation–π coupling interaction between Ppy and *f*-MWCNTs, which can take advantage of the synergic effect of higher electronic conductivity of *f*-MWCNTs and superior catalytic activity of Ppy. This can reduce the internal series resistance and enhance FF and J_{sc} values, which in turn lead to higher conversion efficiency.

Table 2
Parameters of photoelectric performance for the DSSCs with *f*-MWCNTs, Ppy, Ppy/*f*-MWCNT, and Pt on FTO and PEN substrates as the counter electrodes under AM1.5 illumination of 100 mW cm^{-2}.

Counter electrodes	V_{oc} (mV)	J_{sc} (mA cm^{-2})	FF (%)	η (%)
Ppy/FTO	680	12.0	50.2	4.10
f-MWCNTs/FTO	710	8.4	53.4	3.18
Ppy/*f*-MWCNT/FTO	702	16.1	62.1	7.02
Pt/FTO	701	17.4	62.6	7.55
Ppy/*f*-MWCNT/PEN	708	9.3	61.3	4.04
Pt/PEN	710	10.9	61.5	4.76

As the Ppy/*f*-MWCNT film was fabricated at room temperature, flexible DSSCs can be assembled by using PEN substrates, which is a major concern for the application of Ppy/*f*-MWCNT films. The composite film coated on PEN substrate exhibits stronger adhesion against mechanical scratching and bending, as shown in the inset of Fig. 8. As can be seen from Fig. 8, the variation in the performance parameters for the flexible Ppy/MWCNT and Pt counter electrodes is similar to that in the case of FTO substrates counterpart. Although the performance of DSSCs with the Ppy/*f*-MWCNT (4.04%) is slightly lower than that of DSSCs prepared with typical but expensive Pt counter electrode (4.76%), the efficiency can be further improved by optimizing the film thickness, film preparation, film component and so on.

4. Conclusions

In conclusion, Ppy/*f*-MWCNT films were fabricated by a simple drop casting method on FTO and also PEN substrates, and were used as an efficient catalyst for triiodide ions reduction in DSSCs. Due to the synergic effect of higher conductive *f*-MWCNTs and superior catalytic Ppy, the established Ppy/*f*-MWCNT composite as the efficient counter electrode achieves relatively higher efficiency, which is comparable to that of the conventional Pt counter electrode obtained by sputtering. The main advantage of this method is that the production steps can be carried out under ambient conditions, indicating its potential application in flexible DSSCs. It is strongly believed that our results may expand the scope of low cost, high efficient and flexible DSSCs for practical applications.

Acknowledgements

This work was supported by Singapore NRF-CRP grant on "Nanonets for harnessing solar energy and storage" and also NUS and NTU for providing facilities to carry out the research.

References

[1] M.K. Nazeeruddin, F.D. Angelis, S. Fantacci, A. Selloni, G. Viscardi, P. Liska, S. Ito, B. Takeru, M. Grätzel, J. Am. Chem. Soc. 127 (2005) 16835.
[2] P.J. Li, J.H. Wu, J.M. Lin, M.L. Huang, Z. Lan, Q.H. Li, Electrochim. Acta 53 (2008) 4161.
[3] X.M. Fang, T.L. Ma, G.Q. Guan, M. Akiyama, E. Abe, J. Photochem. Photobiol. A: Chem. 164 (2004) 179.
[4] A. Kay, M. Grätzel, Sol. Energy Mater. Sol. Cells 44 (1996) 99.
[5] X.G. Mei, S.J. Cho, B.H. Fan, J.Y. Ouyang, Nanotechnology 21 (2010) 13037.
[6] G.R. Li, F. Wang, Q.Q. Jiang, X.P. Gao, P.W. Shen, Angew. Chem. Int. Ed. 49 (2010) 3653.
[7] Y. Hu, Z. Zheng, H.M. Jia, Y.W. Tang, L.Z. Zhang, J. Phys. Chem. C 112 (2008) 13037.
[8] M. Biancardo, K. West, F.C. Krebs, J. Photochem. Photobiol. A: Chem. 187 (2007) 395.
[9] C.P. Lee, P.Y. Chen, R. Vittal, K.C. Ho, J. Mater. Chem. 20 (2010) 2356.
[10] H.C. Sun, Y.H. Luo, Y.D. Zhang, D.M. Li, Z.X. Yu, K.X. Li, Q.B. Meng, J. Phys. Chem. C 114 (2010) 11673.
[11] D.W. Hatchett, M. Josowicz, Chem. Rev. 108 (2008) 746.
[12] J.H. Wu, Q.H. Li, L.Q. Fan, Z. Lan, P.J. Li, J.M. Lin, S.C. Hao, J. Power Sources 181 (2008) 172.
[13] G.Z. Chen, M.S.P. Shaffer, D. Coleby, G. Dixon, W.Z. Zhou, D.J. Fray, A.H. Windle, Adv. Mater. 12 (2000) 522.
[14] M. Alvaro, C. Aprile, B. Ferrer, H. Garcia, J. Am. Chem. Soc. 129 (2007) 5647.
[15] J.M. Pringle, V. Armel, D.R. MacFarlane, Chem. Commun. 46 (2010) 5367.
[16] L.P. Zhao, Y.J. Li, Z.F. Liu, H. Shimizu, Chem. Mater. 22 (2010) 5949.
[17] H. Asadollahzadeh, E. Noroozian, S. Maghsoudi, Anal. Chim. Acta 669 (2010) 32.
[18] H.F. Guo, H. Zhu, H.Y. Lin, J.Q. Zhang, Colloid. Polym. Sci. 286 (2008) 587.
[19] S.J. Peng, J.F. Shi, J. Pei, Y.L. Liang, F.Y. Cheng, J. Liang, J. Chen, Nano Res. 2 (2009) 484.
[20] S.J. Peng, F.Y. Cheng, J.F. Shi, J. Liang, Z.L. Tao, J. Chen, Solid State Sci. 11 (2009) 2051.
[21] K.C. Huang, Y.C. Wang, R.X. Dong, W.C. Tsai, K.W. Tsai, C.C. Wang, Y.H. Chen, R. Vittal, J.J. Lin, K.C. Ho, J. Mater. Chem. 20 (2010) 4067.
[22] M.X. Wu, X. Lin, T.H. Wang, J.S. Qiu, T.L. Ma, Energy Environ. Sci. 4 (2011) 2308.
[23] J.S. Jang, D.J. Ham, E. Ramasamy, J. Lee, J.S. Lee, Chem. Commun. 46 (2010) 8600.
[24] Y. Saito, W. Kubo, T. Kitamura, Y. Wada, S. Yanagida, J. Photochem. Photobiol. A: Chem. 164 (2004) 153.
[25] E. Ramasamy, W.J. Lee, D.Y. Lee, J.S. Song, Electrochem. Commun. 10 (2008) 1087.
[26] K. Kitamura, S. Shiratori, Nanotechnology 22 (2011) 195703.
[27] R.R. Jia, J.Z. Chen, J.H. Zhao, J.F. Zheng, C. Song, L. Li, Z.P. Zhu, J. Mater. Chem. 20 (2010) 10829.